Journal of *Marine Science and Engineering*

MDPI

Article

Copepod Feeding Responses to Changes in Coccolithophore Size and Carbon Content

Jordan Toullec [1,*], Alice Delegrange [1,2], Adélaïde Perruchon [1], Gwendoline Duong [3], Vincent Cornille [1], Laurent Brutier [1] and Michaël Hermoso [1]

[1] Laboratoire d'Océanologie et de Géosciences—UMR 8187 LOG, CNRS, Université Littoral Côte d'Opale, F-62930 Wimereux, France
[2] Institut national supérieur du professorat et de l'éducation, Académie de Lille—Hauts de France, F-59658 Villeneuve d'Ascq, France
[3] Laboratoire d'Océanologie et de Géosciences—UMR 8187 LOG, CNRS, Université de Lille, F-59000 Lille, France
* Correspondence: toullec.jordan@gmail.com

Abstract: Phytoplankton stoichiometry and cell size could result from both phenology and environmental change. Zooplankton graze on primary producers, and this drives both the balance of the ecosystem and the biogeochemical cycles. In this study, we performed incubations with copepods and coccolithophores including different prey sizes and particulate carbon contents by considering phytoplankton biovolume concentration instead of chlorophyll *a* level (Chl *a*) as is usually performed in such studies. The egestion of fecal pellet and ingestion rates were estimated based on a gut fluorescence method. The latter was calibrated through the relationship between prey Chl *a* level and the biovolume of the cell. Chl *a*/biovolume ratio in phytopkanton has to be considered in the copepod gut fluorescent content method. Both coccolithophore biovolume and particulate inorganic/organic carbon ratios affect the food foraging by copepods. Finally, we observed a non-linear relationship between ingestion rates and fecal pellet egestion, due to the presence of calcite inside the copepod's gut. These results illustrate that both prey size and stoichiometry need to be considered in copepod feeding dynamics, specifically regarding the process leading to the formation of fecal pellets.

Keywords: coccolithophore; elemental stoichiometry; copepods; gut content; ingestion rate; fecal pellet egestion; functional response

Citation: Toullec, J.; Delegrange, A.; Perruchon, A.; Duong, G.; Cornille, V.; Brutier, L.; Hermoso, M. Copepod Feeding Responses to Changes in Coccolithophore Size and Carbon Content. *J. Mar. Sci. Eng.* **2022**, *10*, 1807. https://doi.org/10.3390/jmse10121807

Academic Editors: Marco Uttieri, Ylenia Carotenuto, Iole Di Capua and Vittoria Roncalli

Received: 28 October 2022
Accepted: 17 November 2022
Published: 23 November 2022

1. Introduction

By absorbing about 50% of carbon dioxide (CO_2) from the atmosphere, the Ocean plays a major role in the global carbon cycle [1]. The biological carbon pump is sustained by photosynthetic CO_2 fixation by phytoplankton, and by the transfer of both organic and inorganic carbon to the deep sea [2,3]. Zooplankton, as primary consumers, control the carbon transfer through excretion/respiration [4,5] producing fecal pellets that foster the export of particulate carbon flux, as observed through the analysis of sediment traps [4,6–8].

Mesozooplankton (>200 µm) prey assemblages are constituted of heterotrophic microzooplankton (flagellates, cilliates) and autotrophs such as diatoms and coccolithophores [9–11]. Coccolithophores are a key food-source group widely dispersed throughout the world's oceans [12,13]. They produce calcified structures—coccoliths, which have formed a substantial proportion of pelagic sediments since the Late Triassic period (about 200 million years ago). Fossil records show that coccolithophores were a major component of primary producers over this period, and a significant food source for zooplanktonic grazers during this period [14,15].

Both phytoplankton and zooplankton are the first to experience natural environmental shifts such as phenological changes, or anthropogenic changes induced by global warming or ocean acidification [16]. Recently, morphological changes (cell size and shape) and the

relative abundance distribution in diatom assemblage were linked to the annual phenology in the North Sea [17]. These findings could have consequences on copepod grazing [18–20]. Indeed, morphological defence of phytoplankton against grazing can be the formation of chain, cell size/shape, and biomineralization [21]. Even though copepods are well designed to break down biomineral structures and sometimes can graze on larger prey than themselves [22,23], diatom frustules limit copepod grazing [24–26] as well as microzooplankton grazing [27]. Moreover, it has been established that grazers could induce diatom silicification [28,29], proving the defensive role of the these biomineral structures. Similarly, coccolithophore build biomineral shells made of calcium carbonate (coccoliths) whose formation is influenced by environmental conditions (see reference above). As for diatom frustules, these coccoliths arranged around the cell forming the coccosphere provide mechanical protection [30], and could play a defensive role against microzooplankton grazing [31,32]. Although suggested, but never demonstrated, this calcified coccosphere could also be considered as an anti-grazing protection against copepods [33–35].

Copepods are characterised by distinct functional feeding traits (they are feeding-current feeders or ambush feeders), and as such, are interesting organisms for studying the trophodynamics towards phytoplankton [36]. Classically, ingestion rates increase with food availability and follow Ivlev's model curves [37]. This relationship is formalised by an optimal foraging theory [38,39]. The modification of copepods feeding behaviour potentially has consequences for the functioning of ecosystems, such as "trophic cascades" with consequences on biogeochemical cycles [33,40–42]. In the context of global warming and ocean acidification, a species-specific difference in coccolithophore response is expected [43] on both cell size and calcification. In this study, the modification of calcite content and cell size on copepod ingestion was explored. As a result of experimental incubations, the prediction of an optimal foraging model (Ivlev's model) was tested through direct observations of copepods' functional responses with different coccolithophore species, characterized by different calcite contents and sizes. Moreover food type and availability affect fecal pellet production rates, pellet volumes, and sinking rate, regarding compactness and mineral ballasting [44,45] (Table 1). We hypothesise that both calcite content and prey volume affect copepod functional responses and by this way, the fecal pellet egestion.

Table 1. Parameters indicating the initial conditions during the experimental incubations (mean ± SD, N = 3).

Experiment	Prey Type per Incubation Batch	Cell Diameter	Chlorophyll *a* per Cell	Organic Carbon per Cell	Inorganic Carbon per Cell	Organic Nitrogen per Cell	TPC/N	POC/N	PIC/POC
		[µm]	[pg Chl *a* cell^{-1}]	[pg POC cell^{-1}]	[pg PIC cell^{-1}]	[pg PON cell^{-1}]	[mol:mol]	[mol:mol]	[mol:mol]
1	*G. oceanica*	6.7 ± 0.9	0.16 ± 0.05	13	50.7	4.4 $^{<dl}$	17.0 ^{ns}	3.5 ^{ns}	3.9
	G. oceanica + *Tisochrysis* sp.	6.3 ± 0.9 ^{a}	0.40 ± 0.05 ^{a}	25.8	17	2.6 $^{<dl}$	19.3 ^{ns}	11.6 ^{ns}	0.7
	Tisochrysis sp.	6.1 ± 0.6	0.6 ± 0.1	21.4	0	1.3 $^{<dl}$	19 ^{ns}	19.0 ^{ns}	0
2	*G. oceanica*	6.3 ± 0.9	0.17 ± 0.05	21.5 ± 1.3	6.7 ± 1.4	2.5 ± 0.1	13.3 ± 0.8	10.1 ± 0.3	0.3 ± 0.1
3	*E. huxleyi*	4.5 ± 0.5	0.10 ± 0.01	7.7 ± 0.3	5.4 ± 3.2	1.3 ± 0.2 $^{<dl}$	12.1 ± 4.3 ^{ns}	6.9 ± 0.8 ^{ns}	0.7 ± 0.4 ^{ns}
4	*C. braarudii*	17 ± 2	3.5 ± 0.5	110 ± 7	183 ± 3	13.4 ± 0.8	25.6 ± 1.2	9.7 ± 0.7	1.7 ± 0.1
5	*E. huxleyi*	5.13 ± 0.03	0.12 ± 0.01	20 ± 1	2.6 ± 1.2	1.7 ± 0.1	15.8 ± 1.3	13.9 ± 0.3	0.13 ± 0.07

^{a} Corresponding to the mix of both cell species. $^{<dl}$ Under the detection limit. ^{ns} Statistically non-significant.

2. Methods and Materials

2.1. Phytoplankton Cultures

For the laboratory experiment setup, three species of calcifying Haptophyceae were used: *Emiliania huxleyi* (strain RCC 1256); *Coccolithus braarudii* (strain RCC 1200); and *Gephyrocapsa oceanica* (strain RCC 1314). They were grown in polycarbonate flasks in 100–400 mL of K/2 + Si media at 15 °C and under a 12:12 h day:night photoperiod (100–150 µE m^{-2} s^{-1}). The culture media were prepared with 0.2 µm filtered seawater (FSW) from the English Channel (33–34 PSU) [46]. The culture media pH was adjusted to 8.2 (total scale) by the addition of NaOH. The cells were maintained in an exponential growth phase by renewing the media every week. In parallel, non-calcifying Haptophyceae species were also cultured, *Tisochrysis* sp. (strain RCC 1350), grown inside a 2 L Erlenmeyer flask with a K/2 + Si medium at 15 °C and under a 12:12 h day:night photoperiod (100–150 µE m^{-2} s^{-1}). These cultures were directly used after dilution with 1 µm of FSW buffered at pH 8.2 for the copepod incubation experiments (Table 1).

2.1.1. Cell Count and Size Measures

Cell numeration and sizing were done using a Beckman Coulter Counter Multisizer 4E apparatus fitted with a 70 µm aperture tube. Sampled cell suspensions were diluted with an isotonic (ISOTON II) solution before being analysed. Cell sizes (cell diameter in µm) were determined by the Gaussian distribution of dominant particles present inside the culture samples (containing phytoplankton) (Table 1).

2.1.2. Cell Chlorophyll *a* (Chl *a*) Content

Amounts of 100 mL of pre-diluted phytoplankton culture were filtered onto pre-combusted (4 h at 450 °C) glass fibre filters (Whatman GF/F) and conserved at −20 °C prior to pigment extractions. The filters were then ground overnight in 6 mL of acetone (90%) for chlorophyllian pigment extraction (Chl *a* and phaeopigments) in the dark at 4 °C. Fluorescence of the extract was measured before and after acidification with 10% HCl using a fluorometer (Turner design Trilogy). Results are expressed in pg Chl a_{eq} $cell^{-1}$ (Table 1).

2.1.3. Particulate Inorganic Carbone (PIC), Particulate Organic Carbon (POC), and Particulate Organic Nitrogen (PON)

Before each incubation, 100 mL phytoplankton culture suspensions (with known cell concentration) were filtered onto pre-combusted (4 h at 450 °C) glass fibre filters (Whatman GF/F). All the filters were then rinsed with 10 mL of FSW. Due to the large number of samples, the filters were not triplicated. The filters were placed inside aluminium foil, dried at 55 °C for 24 h, and analysed for elemental C and N using a Thermo Fisher Flash 2000 elemental analyser [47]. Two batches of glass filters were filtered for each sample, one batch with an acid treatment (providing the POC content) and the other without an acid treatment (providing the PIC + POC content), namely the total particulate carbon content, (TPC). PIC was obtained by subtracting POC from the TPC. The results are expressed in mass per cell (pg $cell^{-1}$), for inorganic carbon, organic carbon, and organic nitrogen (Table 1).

2.2. Copepod Sampling

For the laboratory experiments, two calanoid copepod species (*Temora longicornis* and *Acartia* clausi) were selected due to their abundance in the Eastern English Channel (EEC). Their presence generally matches phytoplankton spring blooms in the coastal areas of the EEC [48]. Each species also exhibits different functional traits [49] regarding their feeding strategies: *A. clausi* (1.1 mm total length) is an omnivorous feeding-current feeder with a clear tendency to herbivory; and *T. longicornis* (1.2 mm total length) is described as both a feeding-current feeder and cruise feeder [49,50].

The copepods were collected from February to May 2021 close to the French coast of the EEC (50°44′27.5 N: 1°34′32.4 E) during cruises on-board the N/O Sepia II (INSU-CNRS) with a WP2 plankton net (200 µm mesh size) fitted with a 2 L filtering cod-end

during horizontal net tows (speed < 1 m s^{-1} for less than 10 min) at 1–3 m depth. After each plankton haul, zooplankton samples were immediately diluted in 20 L of surface seawater, then stored in the dark in a cool box and brought back within a few hours to the laboratory. To initiate the rearing phase, a ratio of 1 male per 5 females for calanoid copepods is required [51,52], and this was ensured by selecting about 250 adults of each species under a dissecting microscope. The copepods were placed in polycarbonate beakers of varying volume (from 3 to 7 L according to the number of individuals) containing 1 µm FSW. The copepods were kept at 15 °C, at a salinity of 33–34 PSU and under a 12:12 h day:night photoperiod. They were fed daily under replete food condition. The food supplied consisted of a mixture of microalgae *Rhodomonas salina* (RCC 1507), *Thalassiosira weissflogii* (RCC 1714), *Tisochrysis* sp. (RCC 1350), *Tetraselmis suesica* (RCC 1975), and *Emiliania hyxleyi* (RCC 1256), grown inside a 2 L Erlenmeyer flask with K/2 + Si medium at 15 °C and under a 12:12 h day:night photoperiod (100–150 µE m^{-2} s^{-1}). The media were prepared with autoclaved 1 µm FSW from the EEC. The algal concentrations inside the beakers were from 10^3 to 10^4 cell mL^{-1} [51–53] in order to avoid predation of calanoid copepods on younger stages [54,55]. Seawater was renewed every two days and air was supplied via small bubbles in each rearing beaker.

2.3. Experimental Setup

A total of eleven separate incubations of copepods (each conditions triplicated) were conducted, spread over five assays that allowed the integration of variable predator/prey size ratios and concentration ratios. Phytoplankton cell diameter ranged from 4.5 to 17 µm (Table 1) and concentrations from 1.6 ± 0.2 × 10^3 cell mL^{-1} to 58 ± 2 × 10^3 cell mL^{-1} (Table 2). The corresponding initial food concentrations ranged from 0.49 ± 0.06 to 10.1 ± 2.2 µg Chl *a* L^{-1} and the total cell volume ranged from 0.39 ± 0.03 to 5.55 ± 0.25 mm^3 L^{-1} considering the cell concentrations and their respective cell biovolume, assuming spherical cells (Table 2).

2.3.1. Copepod Selection

For each incubation, adults and copepodite 5 stage were selected corresponding to a mean length of 1097 ± 108 µm (N = 296) and 1216 ± 135 (N = 369) for *Acartia clausi* and *Temora longicornis*, respectively. In order to obtain a significant grazing signal index, copepod abundance inside bottles was high relative to calanoid copepod abundances commonly measured during phytoplankton blooms in the North Atlantic Ocean (typically 4 ind L^{-1} for calanoid copepods such as *T. longicornis, A. clausi* [56]). However, the chosen experimental copepod abundance was comparable to abundances observed in the EEC (up to 11 ind L^{-1}, see Table 2) [57]. These high abundances remained also comparable to values used in most experimental studies ranging from 8 to >15 ind L^{-1} [52,58–60].

2.3.2. Incubation

Twenty-four hours prior to the start of the experiments, 100 reared copepods were isolated in 3 L beakers containing 1 µm FSW without food. This starving phase allowed gut evacuation and maximized the feeding during the incubations. For all experiments, dead and injured individuals were first removed and only healthy-looking and living ones were individually pipetted into a 2350 mL polycarbonate bottle containing prey assemblages. Then, to avoid air bubble introduction the bottles were filled without headspace with FSW adjusted to pH 8.2, and then placed on a rolling table at 3 rpm to allow prey homogenization. Incubation was carried out at 15 °C under a photoperiod regime (12:12 h) for 24 h.

Table 2. Initial grazing experiment incubation setup (mean ± SD, N = 3).

Experiment	Food	Copepod Species	Copepod per Incubation	Replicat	Cell Concentration	Chlorophyll *a* Concentration	Particulate Organic Carbon Concentration	Particulate Inorganic Carbon Concentration	Particulate Organic Nitrogen Concentration
			[ind L^{-1}]	[N]	[10^3 cell mL^{-1}]	[µg Chl *a* L^{-1}]	[µg POC L^{-1}]	[µg PIC L^{-1}]	[µg PON L^{-1}]
1	*G. oceanica*	*T. longicornis*	13–14	3	2.9 ± 0.2	0.5 ± 0.1	37	146	13 $^{<dl}$
	G. oceanica + *Tisochrysis* sp.		13–15	3	3.5 ± 0.3	1.4 ± 0	91	60	9 $^{<dl}$
	Tisochrysis sp.		12–14	3	3.3 ± 0.3	2.0 ± 0.2	72	0	4 $^{<dl}$
2	*G. oceanica*	*A. clausi* *T. longicornis*	11 11	3 3	19.2 ± 0.1	3.2 ± 0.6	441 ± 25	128 ± 27	47 ± 1
3	*E. huxleyi* (low concentration)	*A. clausi* *T. longicornis*	11–14 11–13	3 3	13.7 ± 0.8	1.4 ± 0	104 ± 4	73 ± 43	18 ± 3 $^{<dl}$
4	*C. braarudii*	*A. clausi* *T. longicornis*	14–18 11–17	3 3	2.2 ± 0.9	7.6 ± 0.2	244 ± 16	405 ± 7	30 ± 2
5	*E. huxleyi* (high concentration)	*A. clausi* *T. longicornis*	16–19 11	3 3	57.9 ± 0.2	7.3 ± 0.4	1157 ± 57	151 ± 69	97 ± 7

$^{<dl}$ Under the detection limit.

2.4. Ingestion/Egestion Estimation

After each incubation, the copepods were carefully retrieved from each bottle by sieving the seawater through an immersed 200 µm mesh. The copepods were placed in 2 mL cryotubes (one per bottle) and then flash frozen in liquid nitrogen and kept at –20 °C until further analysis. Copepod size measurements were performed (as much as possible not withstanding obscurity) under a dissecting microscope (ZEISS Axio Zoom V16), before pigment extraction for gut content quantification (see below). Fecal pellets were recovered after each incubation by filtering the remaining seawater of each bottle onto a 40 µm mesh sieve. Fecal pellets retained on the mesh sieve were resuspended in FSW in a plankton counting chamber (Dolfuss cuvette, 6 mL volume).

2.4.1. Copepod Gut Pigment Content

For gut content analyses, copepods were individually sorted from freshly thawed samples under a cool light stereomicroscope. Individuals were rinsed with 0.2 µm FSW to eliminate phytoplankton cells with aggregates stuck to feeding appendages and were then transferred into 4 mL acetone (90%). Individuals (N = 19 to 42 copepods per extraction) were ground and chlorophyllian pigments (Chl *a* and phaeopigments) were extracted in the dark at 4 °C overnight. Fluorescence of the extract was measured before and after acidification with 10% HCl using a fluorometer (Turner design Trilogy). Copepod gut content was obtained by both Chl *a* and phaeopigment concentrations and values were not corrected for pigment degradation on the recommendation of Durbin and Campbell [61]. Ingestion rates (I, ng Chl $a_{\text{ eq}}$ ind^{-1} d^{-1}) were derived from gut total pigment content (G_{cop}, ng Chl $a_{\text{ eq}}$ ind^{-1}) using Equation (1):

$$I = 60 \times G_{cop} \times k \quad (1)$$

where k is the gut evacuation rate (h^{-1}), calculated following the model of Dam and Peterson [62], which accounts for the temperature of incubation, and the specie-dependant allometric constant. In the present study, we carried out our calculations with k = 0.028, which corresponds to the allometric constant of evacuation of calanoids at 15 °C (k = 0.0117 + 0.001794 × T).

2.4.2. Copepod Gut Volume Conversion

Phytoplankton species used during the grazing experimental setup did not have the same biovolume and Chl *a* content (see Table 1). In order to compare every gut content for each experiment, we converted the equivalent pigment gut content (ng Chl $a_{\text{ eq}}$ ind^{-1}) into volume equivalent gut content (µm^3 $_{\text{eq}}$ ind^{-1}). A calibration of Chl *a* level (pg Chl a cell^{-1}) over cell biovolume (µm^3) for each phytoplankton species was used. Gut ingestion was then expressed as its prey biovolume equivalent (10^6 µm^3 $_{\text{eq}}$ ind^{-1} d^{-1}).

2.4.3. Ivlev's Model

The copepod ingestion functional response toward food availability was calculated by following Ivlev's model [38,39]—Equation (2). This model considers the optimal food foraged by copepods (and more widely by all planktonic active filter feeders), recently described as a *Type II functional response* [63,64].

$$I_{Ivlev} = I_{max} \times \left(1 - e^{(-\alpha \times C_{food})}\right) \quad (2)$$

where I_{max} is the maximum ingestion rate index obtained; α the rate at which saturation is achieved with increasing food levels (slope of the linear regression); I_{Ivlev} is the modelized ingestion rate; and C_{food} is the corresponding food concentration (µg POC L^{-1}, µg Chl *a* L^{-1} or mm^3 L^{-1}).

2.4.4. Fecal Pellet Production and Size

Fecal pellet production (FP ind^{-1} d^{-1}) was estimated after each experiment by counting the fecal pellets recovered after incubation. For each incubation, between 10 and 186 pellets were measured (length and width in µm) with 5 µm accuracy. Fecal pellets are considered as cylindrical with two half spheres, and volumes were calculated according to Equation (3) [65]:

$$V_{PF} = \pi \times d^2 \times \left(\frac{L}{4} + \frac{d}{6}\right) \quad (3)$$

where d is the pellet diameter (µm), and L is the length of cylindric part of the pellet. Volumes were then converted into equivalent spherical diameter (ESD, mm), according to Equation (4):

$$ESD = \sqrt[3]{\frac{6 \times V}{\pi}} \quad (4)$$

2.5. Statistical Analyses

Results are expressed in mean ± standard deviation (SD). When data distribution matched the parametric assumption of normality (tested with a Shapiro–Wilk test, $p < 0.05$), correlation between two variables was analysed using a Pearson correlation test. Otherwise, a Spearman rank correlation test was performed. The statistical effect of the different experimental conditions was tested with a one-way ANOVA, followed by a pairwise Tukey's *post hoc* comparison test. In case of non-normal distribution, multicomparaisons were performed using the Kruslal–Wallis test following Nemeyi *post hoc* test. All the statistical analysis was performed using R software (V 4.1.1).

3. Results

3.1. Coccolithophore Stochiometry

Cellular particulate organic carbon (pg POC cell^{-1}), nitrogen (pg PON cell^{-1}), and inorganic carbon (pg PIC cell^{-1}) increase with coccolithophore diameter (Table 1). Cellular content and stoichiometric ratios for each experiment and coccolithophore species are also presented in Table 1. The cells are considered as spheres, whose biovolumes varied from 38 to 83 µm^3 for *E. huxleyi* (RCC 1256), from 133 to 143 µm^3 for *G. oceanica* (RCC 1314), and from 2296 to 2487 µm^3 for *C. braarudii* (RCC 1200).

3.2. Copepod Ingestion

For experiment 1, a mixture of coccolithophores (*G. oceanica*, RCC 1314) and non-coccolithophores (*Tisochrysis* sp. RCC 1350) was incubated with the copepods (*T. longicornis*). These two haptophyte species have similar sizes (6.7 µm and 6.1 µm of diameter for *G. oceanica* and *Tisochrysis* sp., respectively). They were mixed to obtain three batches: 100% *G. oceanica*, 50% *G. oceanica* + 50% *Tisochrsis* sp., and 100% *Tisochrysis* sp. with approximately 3000 cell mL^{-1} in total (see Table 2). The cell density (cell mL^{-1}) and total cell volume (mm^3 L^{-1}) were non-significantly different between the three different conditions (Figure 1A) with an average of 3255 ± 292 cell mL^{-1} and 0.44 ± 0.04 mm^3 L^{-1}, respectively. Concerning the Chl *a* concentration, *G. oceanica* incubation contained 0.49 ± 0.06 µg Chl *a* L^{-1}, mix of *G. oceanica* and *Tisochrysis* sp. contained 1.40 ± 0.01 µg Chl *a* L^{-1}, and *Tisochrysis* sp. contained 2.04 ± 0.17 µg Chl *a* L^{-1} (Figure 1C). Particulate matter composition (µg POC, PIC, and PON L^{-1}) was achieved within the three different conditions (Figure 1D) and is presented in Table 2.

The resulting ingestion rates varied from 0 (under detection limit) to 13.1 ± 1.4 ng Chl *a* $_{eq}$ ind^{-1} d^{-1} with the higher values encountered in the 100% *Tisochryisis* sp. condition. Volume equivalent ingestion rates (Table 1, Figure 2B) varied from 0 (under the detection limit) to higher values for incubation with *Tisochrysis* sp (2.5 ± 0.3 × 10^6 µm^3$_{eq}$ ind^{-1} d^{-1}). The egestion rates were not significantly different between conditions, with averaged values of 26 ± 7 fecal pellets in d^{-1}, and mean pellet volumes ranging significantly from 0.3 ± 0 with *G. oceanica*, to 1.6 ± 0.6 mm^3 with *Tisochrysis* sp. (Figure 2D).

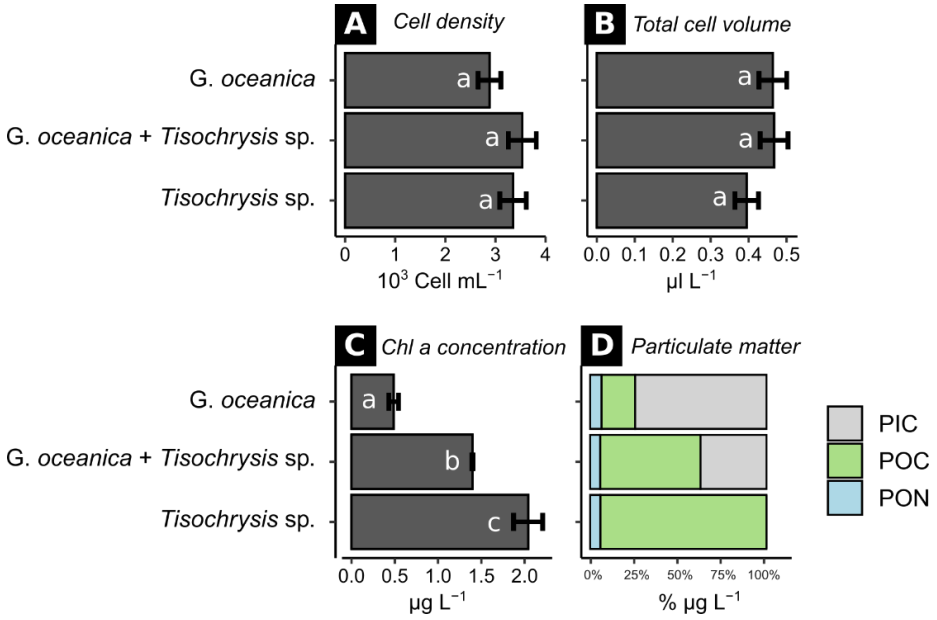

Figure 1. Experiment 1 incubations with *Temora longicornis*. (**A**) Initial cell density for each condition. (**B**) Initial cell volume for each condition for each condition. (**C**) Initial Chl *a* concentration for each condition. (**D**) Initial particulate matter quality for each condition. Groups a, b, and c correspond to statistical groups, according to one-way ANOVA with significant threshold $\alpha = 5\%$ (p-value < 0.05).

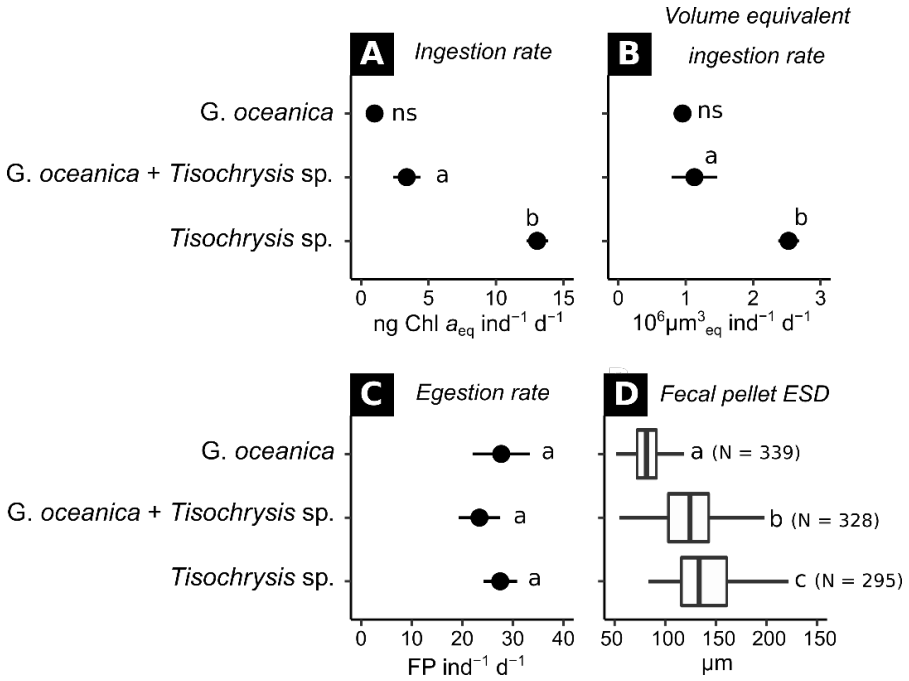

Figure 2. Details of Experiment 1 incubations with *Temora longicornis*. (**A**) Ingestion rate for each condition. (**B**) Volume equivalent ingestion rate for each condition. (**C**) Egestion rate for each condition. (**D**) Fecal pellet equivalent spherical diameter (ESD). Group a, b, and c correspond to statistical group, according to one-way ANOVA with significant threshold $\alpha = 5\%$ (p-value < 0.05). ns = non-significant.

After the incubations, the recovered fecal pellets had both significantly different sizes (Figures 2D and 3) and different opacity: when copepods were fed with 100% *G. oceanica*, fecal pellets were opaque and thick whereas they were light green with *Tisochrysis* sp. Fecal

pellets had an intermediate aspect where the copepods were fed with a mix of both species (Figure 3).

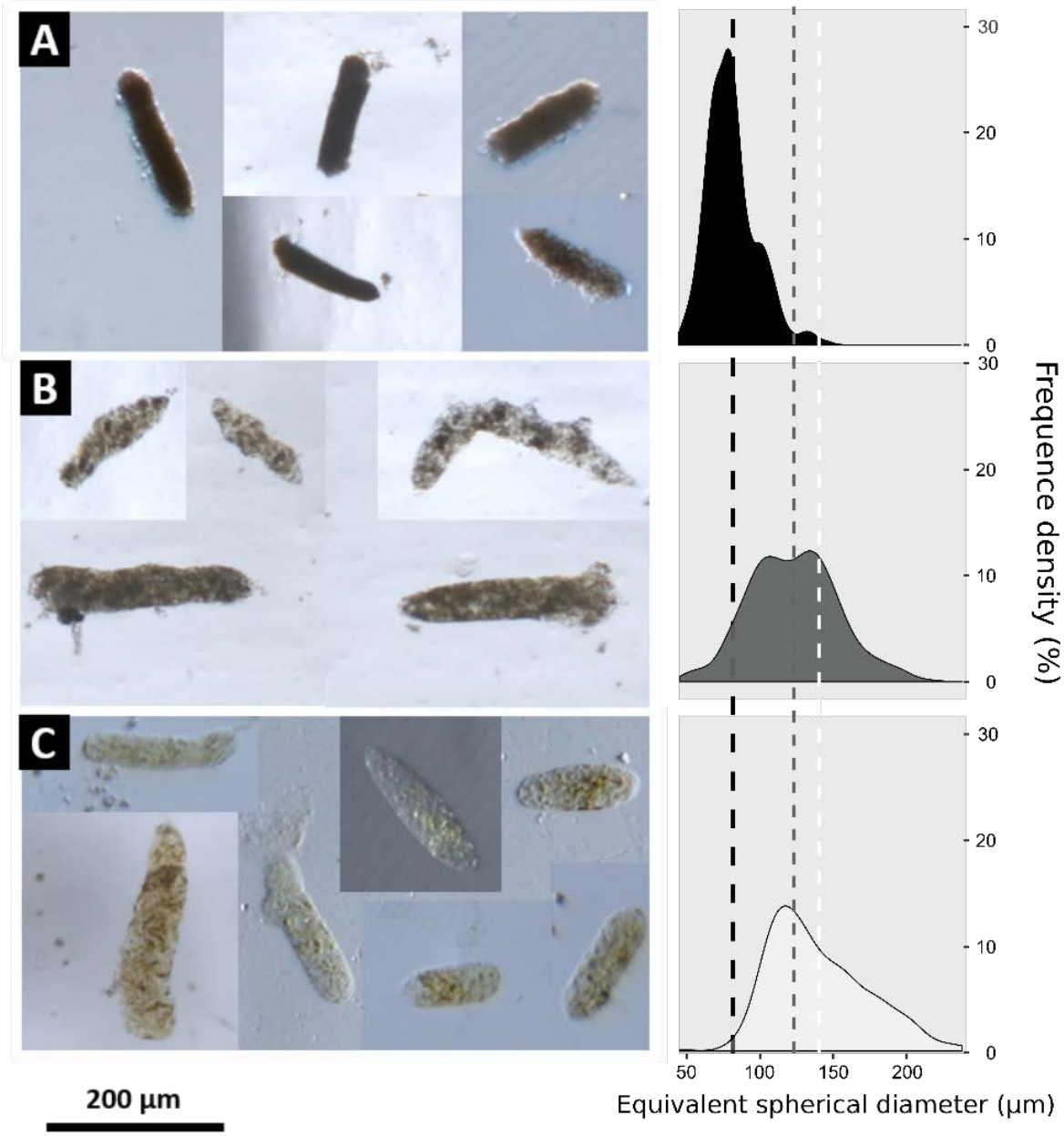

Figure 3. Picture of the recovered *Temora longicornis* fecal pellets of Experiment 1, after different conditions: (**A**) grazing experiment with 100% *G. oceanica*; (**B**) Grazing experiment with a mixture of 50% *G. oceanica* + 50% *Tisochrysis* sp.; and (**C**) Grazing experiment with *Tisochrysis* sp. The scale bar is congruent with figure (**A**–**C**). The vertical black dashed line corresponds to the mean fecal pellet diameters (µm) recovered after grazing experiment with 100% *G. oceanica* (**A**); the vertical grey dashed line corresponds to the mean fecal pellet diameters (µm) recovered after grazing experiment with a mixture of 50% *G. oceanica* + 50% *Tisochrysis* sp (**B**); the vertical white dashed line corresponds to the mean fecal pellet diameters (µm) recovered after grazing experiment with *Tisochrysis* sp (**C**).

The following figures (Figures 4–8) and results consider all the experiments.

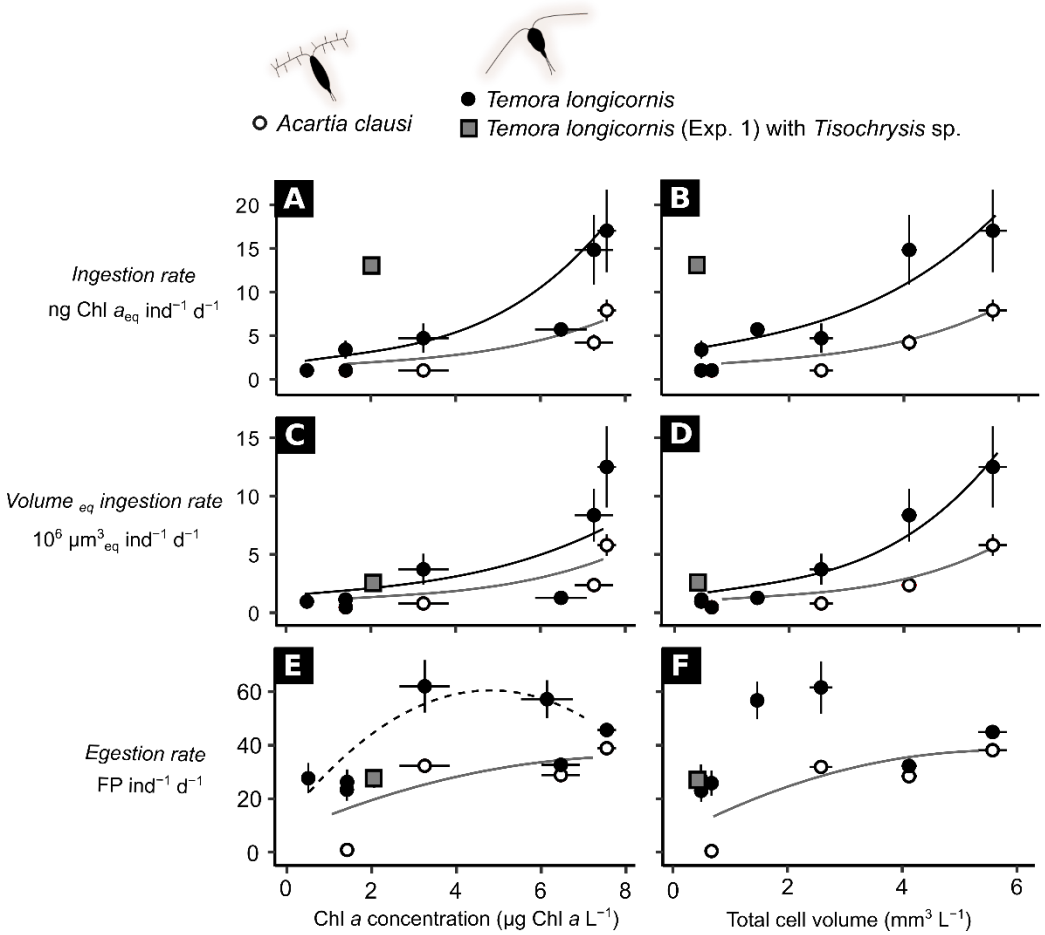

Figure 4. Copepod functional responses over initial Chl *a* concentration (µg Chl *a* L^{-1}) are shown on the left, and over initial total cell volume (mm^3 L^{-1}) are shown on the right. (**A**,**B**) depict the pigment ingestion rate (ng Chl *a* $_{eq}$ ind^{-1} d^{-1}); (**C**,**D**) depict the volume equivalent ingestion rate (10^6 μm^3 $_{eq}$ ind^{-1} d^{-1}); and E and F depict the fecal pellet egestion rate (FP ind^{-1} d^{-1}). Black circular dots correspond to incubation with *Temora longicornis*. White circular dots correspond to incubation with *Acartia clausi*. Grey square dots correspond to incubation with *Temora longicornis* and *Tisochrysis* sp. cell (monospecific and mixed with *G. oceanica*). Solid lines represent exponential fit of pigment/volume equivalent ingestion rate over Chl *a* concentration and total cell volume (**A**–**D**). In (**E**,**F**), solid lines correspond to quadratic fit of fecal pellet egestion over Chl *a* concentration and total cell volume. All equations and statistics are displayed in Table 3. In all graphs, *p*-values < 0.001 are displayed by solid lines, however, *p*-values < 0.05 are displayed by dashed lines (see statistical test in the Methods Section).

The functional responses to prey concentration varied significantly between those copepod species with an average lower ingestion and fecal pellet egestion by *A. clausi* compared to those with *T. longicornis* (Figure 4). Including all experiments, the Chl *a* concentration ranged from 0.49 ± 0.06 to 7.6 ± 0.2 µg Chl *a* L^{-1} (Figure 4A,C,E). The total cell volume ranged from 0.39 ± 0.03 to 5.5 ± 0.3 mm^3 L^{-1} (Figure 4B,D,F). In parallel, the ingestion rate values increased from 0 to 9.9 ng Chl *a* $_{eq}$ ind^{-1} d^{-1} for *Acartia clausi* and from 0 to 23.1 ng Chl *a* $_{eq}$ ind^{-1} d^{-1} for *Temora longicornis* (Figure 4A,B). The volume equivalent ingestion rate values ranged from 0.46 to 7.3 × 10^6 μm^3 $_{eq}$ ind^{-1} d^{-1} for *Acartia clausi* and from 0.9 to 17 × 10^6 μm^3 $_{eq}$ ind^{-1} d^{-1} for *Temora longicornis* (Figure 4C,D). The fecal pellet egestion rate ranged from 4 to 41 FP ind^{-1} d^{-1} for *Acartia clausi* and from 19 to 76 FP ind^{-1} d^{-1} for *Temora longicornis* (Figure 4E,F). All fits and statistical parameters are displayed in Table 3.

Table 3. Regression and statistical parameters within functional relation between food level index and ingestion rate index.

Food Level Index	Grazing Rate Index	Copepod	Statistics	
		T. longicornis	**Equation**	**R^2**
Ingestion rate index			*Exponential fit*	
Chl *a* concentration (μg Chl *a* L^{-1})	Pigment ingestion rate (ng Chl a_{eq} ind^{-1} d^{-1})		$y = 2.2 \times 10^{-5}\ e^{(1.46x)} + 4.49$	0.64 ***
	Volume equivalent ingestion rate (10^6 μm^3_{eq} ind^{-1} d^{-1})		$y = 7.4 \times 10^{-7}\ e^{(2.19x)} + 1.6$	0.67 ***
Total cell volume (mm^3 L^{-1})	Pigment ingestion rate (ng Chl a_{eq} ind^{-1} d^{-1})		$y = 3.1\ e^{(0.31x)} + 0.82$	0.65 ***
	Volume equivalent ingestion rate (10^6 μm^3_{eq} ind^{-1} d^{-1})		$y = 3.02\ e^{(0.29x)} - 2.4$	0.85 ***
Egestion rate index			*Quadratic fit*	
Chl a concentration (μg Chl *a* L^{-1})	Egestion rate (FP ind^{-1} d^{-1})		$y = -2.53x^2 + 24.34x$	0.47 *
Total cell volume (mm^3 L^{-1})			$y = -6.05x^2 + 39.3x$	0.38 ^{ns}
		A. Clausi		
Ingestion rate index			*Exponential fit*	
Chl *a* concentration (μg Chl *a* L^{-1})	Pigment ingestion rate (ng Chl a_{eq} ind^{-1} d^{-1})		$y = 3.9 \times 10^{-8}\ e^{(2.52x)} + 0.99$	0.81 ***
	Volume equivalent ingestion rate (10^6 μm^3_{eq} ind^{-1} d^{-1})		$y = 1.5 \times 10^{-9}\ e^{(2.9x)} + 0.55$	0.78 **
Total cell volume (mm^3 L^{-1})	Pigment ingestion rate (ng Chl a_{eq} ind^{-1} d^{-1})		$y = 0.43\ e^{(0.53x)} + 0.06$	0.85 ***
	Volume equivalent ingestion rate (10^6 μm^3_{eq} ind^{-1} d^{-1})		$y = 0.126\ e^{(0.683x)} + 0.22$	0.85 ***
Egestion rate index			*Quadratic fit*	
Chl a concentration (μg Chl *a* L^{-1})	Egestion rate (FP ind^{-1} d^{-1})		$y = -1.3x^2 + 13.7x$	0.76 **
Total cell volume (mm^3 L^{-1})			$y = -0.84x^2 + 10.9x$	0.87 ***

ns = non-significant, * p-value < 0.05, ** p-value < 0.01 and *** p-value < 0.001, according to Pearson correlation test.

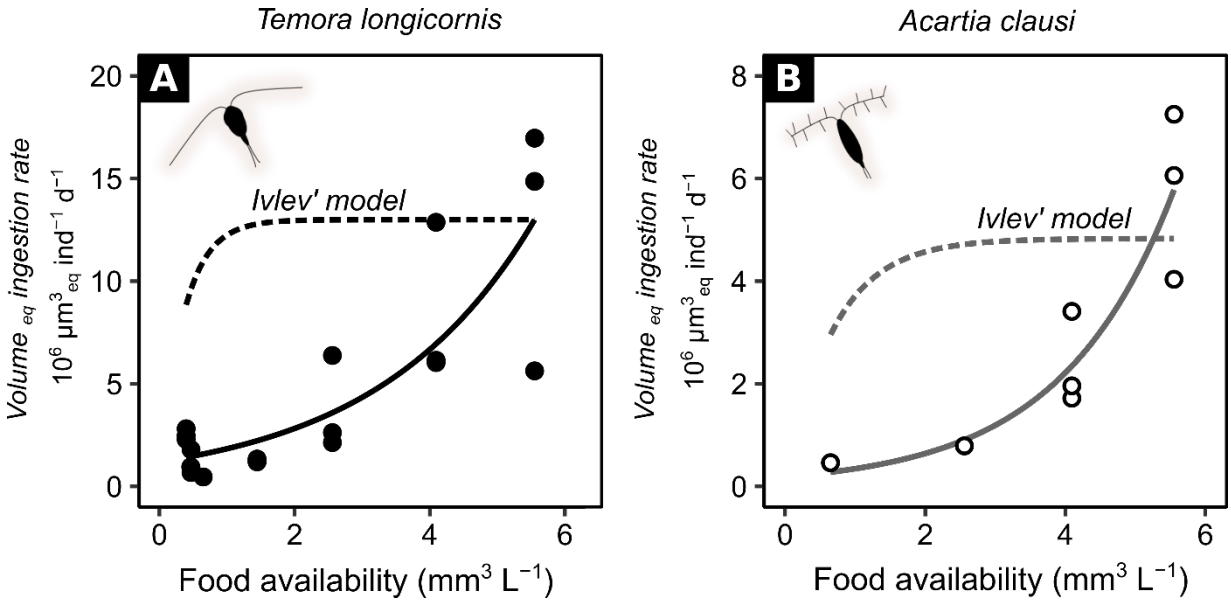

Figure 5. Copepod functional responses over total cell volume (mm^3 L^{-1}), for *Acartia clausi* (**A**) and *Temora longicornis* (**B**). Solid lines represent exponential fit of volume equivalent ingestion rate (10^6 µm^3 $_{eq}$ ind^{-1} d^{-1}) over total cell volume (mm^3 L^{-1}). Dashed lines correspond to Ivlev's model considering the max ingestion rate and the increasing ingestion rate over the food level slope (Equation (2)).

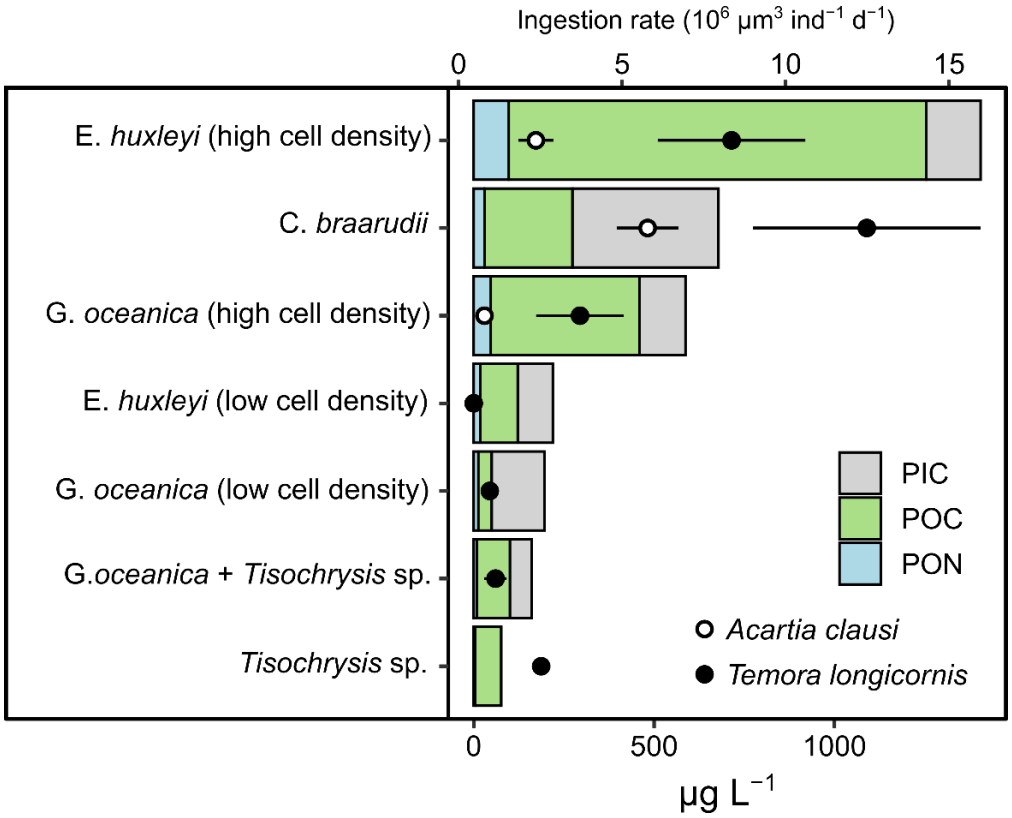

Figure 6. Cumulative barplot of particulate organic nitrogen (PON), particulate organic carbon (POC), and particulate inorganic carbon (PIC) in µg L^{-1} for each experimental incubation (bottom axis). Depicted on the top *x*-axis: the scatterplot of the ingestion rate (10^6 µm^3 $_{eq}$ in^{-1} d^{-1}) with *Acartia clausi* (white dots) and *Temora longicornis* (black dots).

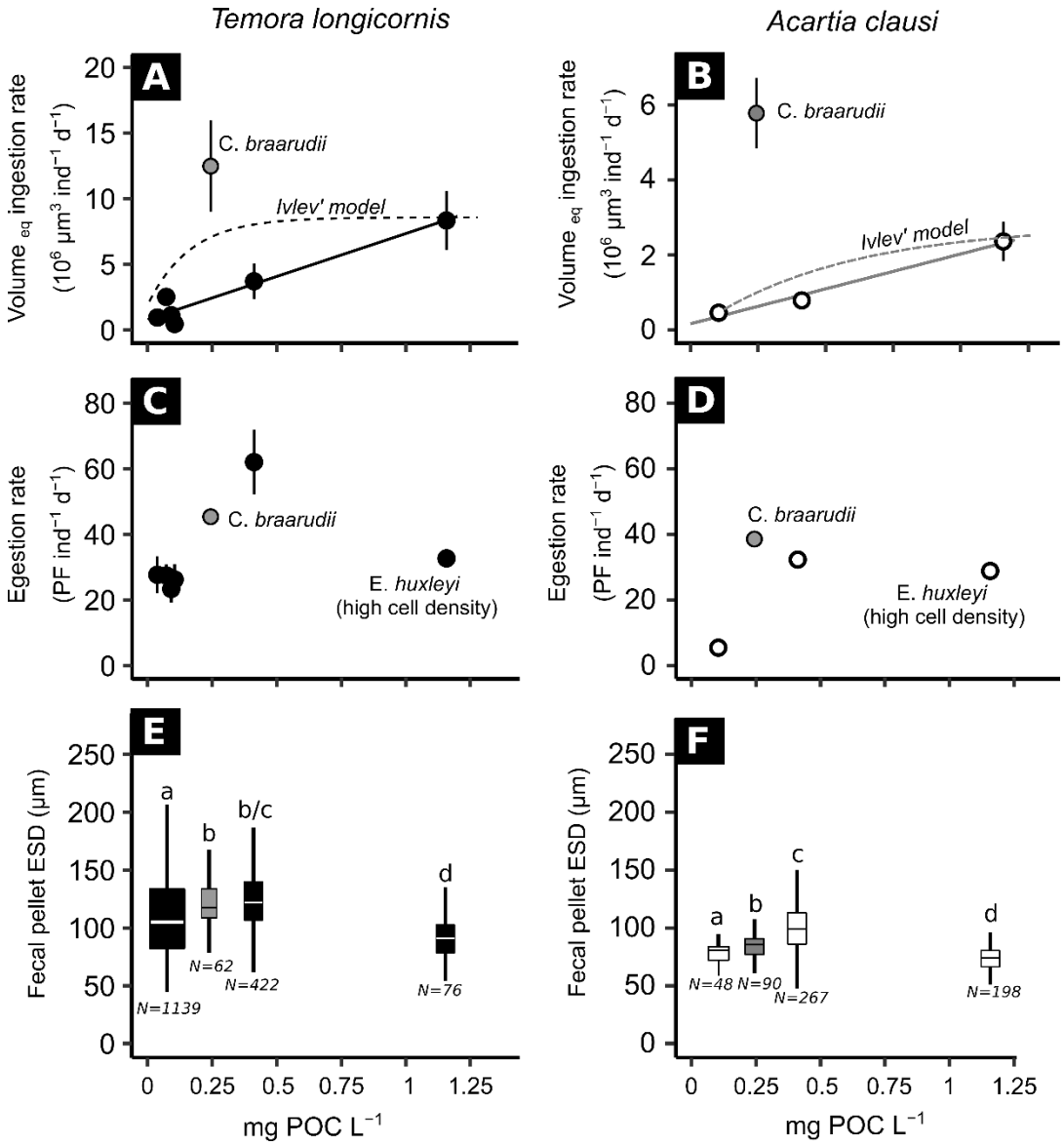

Figure 7. (**A**,**B**) Ingestion rate (10^6 µm^3 $_{eq}$ ind^{-1} d^{-1}); (**C**,**D**) egestion rate (FP ind^{-1} d^{-1}) and (**E**,**F**) fecal pellet ESD (µm) over POC concentration (mg POC L^{-1}) for *Temora longicornis* (**A**,**C**,**E**) and *Acartia clausi* (**B**,**D**,**F**). The grey-boxed dots correspond to Experiment 4 with *C. braarudii*. The solid lines in (**A**,**B**) represent the linear regression between POC concentration and the ingestion rate, excluding the grey circular dot (Experiment 4 with *C. braarudii*). For *T. longicornis*, Pearson R^2 = 0.86, N = 12, *p*-value = 0.001, for *A*. clausi, Pearson R^2 = 0.88, N = 12, *p*-value = 0.002 Dashed lines correspond to Ivlev's model considering the max ingestion rate and the increasing ingestion rate over the food level slope (Equation (2)). Letters a, b, c, and d (in (**E**,**F**)) correspond to the different statistical groups displayed by the Kruskall–Wallis test.

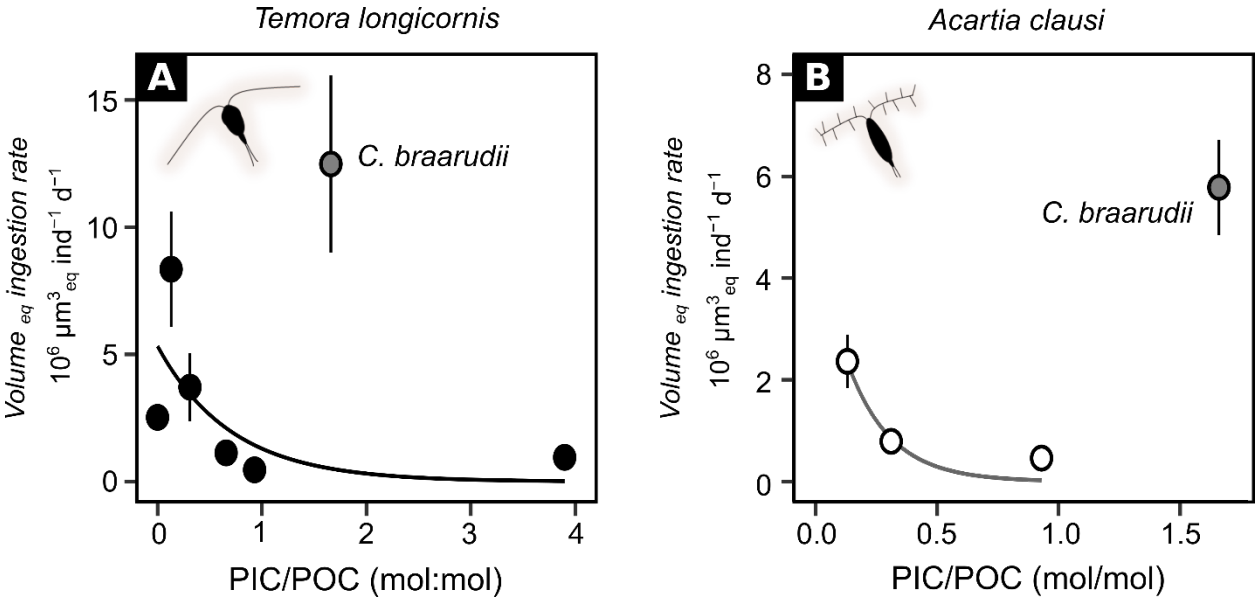

Figure 8. (**A**) Volume equivalent ingestion rate (10^6 µm^3 $_{eq}$ ind^{-1} d^{-1}) over PIC/POC ratios (mol:mol) for incubation with *T. longicornis (Black dots)*; (**B**) volume equivalent ingestion rate (10^6 µm^3 $_{eq}$ ind^{-1} d^{-1}) over PIC/POC ratios (mol:mol) for incubation with *A. clausi* (white dots). Grey dots correspond to incubation with *C. braarudii*. For incubations with *T. longicornis*, Kendall $\tau = -0.59$, N = 18, *p*-value = 0.002, excluding the grey dot (Exp. 4 with *C. braarudii*). For the incubation with *A. clausi*, Kendall $\tau = -0.95$, N = 9, *p*-value < 0.001, excluding the grey dot (Exp. 4 with *C. braarudii*).

The food availability varied between 0.39 ± 0.03 and 5.5 ± 0.3 mm^3 L^{-1}, and the ingestion rate varied from 0.46 to 7.3 × 10^6 µm^3 ind^{-1} d^{-1} for *A. clausi* and from 0.9 to 17.0 × 10^6 µm^3 ind^{-1} d^{-1} for *T. longicornis* (Figures 4 and 5). Exponential fits (solid lines) for both copepods (see Table 3) correspond to *Type III functional response* [63]. The logarithmic fits (dashed lines) were expected (Figure 5), following optimal food foraging (Ivlev's model or *Type II functional response*).

Particulate inorganic carbon (PIC) ranged from 0 (*Tisochrysis* sp. under detection limit) to 433 µg L^{-1} (Figure 6). Particulate organic carbon (POC) ranged from 37 to 1157 µg L^{-1} (Figure 6). Particulate organic nitrogen (PON) ranged from 4 to 97 µg L^{-1} (Figure 6). During Experiment 3 (C. *braarudii*) the PIC concentration represented 55% of the total particulate pool (with 433 µg PIC L^{-1} over 300 µg POC L^{-1} and 55 µg PON L^{-1}). Except for Experiment 5, the copepod ingestion rate increased with increasing ambient particulate content (Figure 6).

When considering all the experiments—except the one with *C. braarudii* (grey dots in Figures 7 and 8)—POC concentration and equivalent volume ingestion rates are positively correlated for both copepod species (*T. longicornis*: y = 0.006x + 0.81; $R^2 = 0.71$; *p*-value < 0.001 Pearson correlation test, and with *A. clausi*: y = 0.002x + 0.17; $R^2 = 0.77$; *p*-value = 0.002 Pearson correlation test). Logarithmic fits were expected following theoretical optimal food foraging (Figures 4, 5 and 7), dashed lines: Ivlev's model or *Type II functional response*. Nevertheless we observed linear regression between POC concentration and equivalent volume ingestion rates which are described in the literature as *Type I functional response* [63]. Fecal pellet egestion ranged from 4 to 41 FP ind^{-1} d^{-1} for *Acartia clausi* and from 19 to 76 FP ind^{-1} d^{-1} for *Temora longicornis* (Figure 7 C,D). Despite a positive correlation between POC concentration and equivalent volume ingestion rates for both copepods, fecal pellet egestion was not correlated to POC concentration (Figure 7C,D). Moreover, within incubations with *T. Longicornis* and *E. Huxleyi* with high cell density (Exp. 5), despite high volume equivalent ingestion rate (8.3 ± 3.9 × 10^6 µm^3 $_{eq}$ ind^{-1} d^{-1}), fecal pellet egestion remained low (32 ± 3 FP ind^{-1} d^{-1}). After incubation with *T. longicornis*,

the mean fecal pellet ESD ranged from 90 ± 17 to 124 ± 25 mm, whereas, after incubation with *A. clausi*, the mean fecal pellet ESD ranged from 71 ± 11 to 97 ± 20 mm.

Variations of cell calcite content were expressed as PIC/POC ratios (mol:mol) for each experiment (see Tables 1 and 2). Volume equivalent ingestion rate (10^6 μm^3 $_{eq}$ ind^{-1} d^{-1}) over PIC/POC ratios (mol:mol) decreased non-linearly for both *T. longicronis* and *A. clausi* (Figure 8), when excluding experiments performed with *C. braarudii*.

4. Discussion

Copepod and more widely zooplankton food foraging is the main prey/predator quantifiable interaction. Within marine planktonic ecosystems, these trophic relationships have direct consequences on population dynamics for both preys and predators [66,67]. Indeed, copepod behavioural adaptations affect both ecological dynamics and biogeochemical cycles, such as primary production and sinking particles fluxes [4,68,69]. Numerical models have shown that copepods could also affect the phytoplankton prey population diversity via a top-down control [70], and also the seasonal succession of plankton communities [19].

4.1. Equivalent Volume Ingestion Estimation

Pigment ingestion rates based on copepod gut fluorescent content [62,71] represent a fast and easy workable way to estimate grazing. Regarding incubation times, which were equivalent in all incubations, pigment destruction inside the gut increased with gut ingestion [72], suggesting that loss of fluorescence is equivalent among the different samples from the different incubations. However, ingested preys could present significant variation in fluorescence, especially in situ; due to ingestion of non-chlorophyllian prostists (ciliates, heterotropic flagellates, nauplii) and algae (diatoms, haptophyceae) in varying proportions. In order to compare the ingestion rates derived from all the experiments (regardless of phytoplankton cell Chl *a* content and their biovolume), we used a conversion of gut content considering Chl *a* and biovolume (see Methods Section). This allowed us to get a better correlation between ingestion and total cell volume (r^2= 0.85 *** for both A. *clausi* and T. *longicornis*, Table 3) than the pigment ingestion rate in accordance to Chl *a* concentration (r = 0.64 *** and 0.81 *** for T. *longicornis* and A. *clausi*, respectively; Table 3, Figure 5). Regarding these findings, we assume that the probability of prey/predator contact is more dependent on total cell volume than the number of particles (cell L^{-1}), or biomass (g Chl *a* L^{-1} or g POC L^{-1}). Thus, it can be assumed that the total cell volume per litre (mm^3 L^{-1}) represents a better index of the prey-encounter rate. This suggests that, at equivalent total cell concentrations, the same ingestion rate pattern, expressed in volume equivalent Chl *a* (μm^3 $_{eq}$ ind^{-1} d^{-1}), could be expected with large cells at low concentration as well as with small cells at high concentration. However, gut analysis neither takes into account pigment degradation inside the copepod's gut [61,72] before ingestion nor sloppy feeding (cell fragmentation without ingestion, see pictures in Jansen, 2008). Considering the very short gut passage time (less than an hour) and the relative evidence of viable cell preservation inside fecal pellets [73,74], the pigment degradation could be neglected (the same condition of sample preservation and treatment).

4.2. Adaptive Functional Response

Classically, the ingestion rate index based on gut content over food availability, which provides Ivlev's model curve [37], represents the optimal foraging behaviour, even regarding incubation time and pigment destruction inside the gut [72]. In this study, both prey/predator size ratios and prey stoichiometry modulate the ingestion rate index. A *Type III functional response* was obtained with both *A. clausi* and *T. longicornis* when considering food availability by total cell volumes and Chl *a* concentration (Figures 5 and 6). Indeed, ingestion rates increased exponentially according to food availability [63,64]. This functional relationship reflects a switching adaptation considering the food quality. The maximum food level reached 5 mm^3 L^{-1}, and is comparable to the maximum food availability in the literature (4 mm^3 L^{-1}) in Kiørboe et al. [64], when the copepod's ingestion saturation

occurs (e.g., *Acartia tonsa*, *Temora longicornis*, *Centropages hamatus*, and *Oithona davisae*). At high food concentration (7.6 ± 0.2 µg Chl *a* L^{-1}), we assume a saturation of the feeding activity. Indeed, with more than 7 µg Chl *a* L^{-1}, the bottles showed green coloration. In our study, we exceeded 5 mm^3 L^{-1} at 15 °C. Thus, performing additional experiments at higher food concentrations would have had no benefit. POC, PIC, and PON quota per cell compare well to those presented in the literature, with a magnitude from 1 to 10^2 pgC $cell^{-1}$ and 10^{-1} to 10 pgN $cell^{-1}$ [75,76]. For both *T. longicornis* and *A. clausi*, the ingestion rates increased linearly with POC concentrations (Figure 7A,B), when excluding experiments with *C. braarudii*, 17 µm diameter. This suggests a *Type I functional response* [63] corresponding to a linear increase of ingestion according to food availability. This is the most common behaviour attributed to planktonic active filter feeders (such as copepods). However, calanoid copepods (such as *Acartia* spp., *Temora* spp., *Centropages* spp., and *Calanus* spp.) commonly present *Type I* and *II* functional responses, mainly corresponding to the Ivlev model [77–80]. Ivlev's model is shaped like *Type II functional response*, which corresponds to the optimal feeding behaviour towards high-quality food availability. In this study, any relationship (either considering Chl *a* concentration, total volume, or POC concentration) fits with Ivlev's model (or *Type II functional response*) suggesting an anti-grazing propriety of the coccolithophores as a food source alone. Within the six incubations with *C. braarudii*, regarding food availability as equivalent carbon, Chl *a* or total volume, we obtained higher ingestion rates than for smaller coccolithophore, which can be explained by an intense gut accumulation of algae material because of the large cell size. Calcite cell content through PIC/POC ratio (mol:mol) for coccolithophore cells of similar sizes (Figure 8) could partially explain a non-optimal ingestion pattern observed in our experiments. These results suggest that the coccosphere (i.e., calcified exosqueletton around the cell) could be a structure protecting the coccolithophore from grazing by copepods, such as diatom frustules, as previously proposed [33,34].

4.3. Calcite Obstruction and Potential Dissolution Inside Copepod Guts

While the copepods ingested large coccolithophore (*C. braarudii*), we measured high ingestion rates despite low carbon concentration and low fecal pellet egestion. This observation indicates a decoupling between ingestion rate and gut passage time [80], probably due to high calcite ingestion and a decrease in gut pH resulting from calcite dissolution. This phenomenon may explain an importance paradox in ocean zooplankton mediated calcite dynamics. Indeed, considering a global oceanic alkalinity budget, there is a loss of calcite between the production by calcifier organisms in the euphotic zone and the estimated calcite flux below the lysocline [81]. This calcite loss could be attributed to biological activities and more specifically the dissolution mediated by zooplankton grazing or transport. Several studies have even shown a loss of calcite after zooplankton gut passage, a striking feature of the sedimentary record that relies on the observation of well-preserved coccoliths within zooplankton fecal pellets [79,82–85]. However, numerical models using a timeframe and pH inside copepod guts suggest a moderate calcite dissolution inside the gut [86]. Langer et al. [87] showed that calcite dissolution during copepod gut passage was below 8% of the weight of the coccoliths of *Calcidiscus leptoporus* inside fecal pellets, but these coccoliths were intact and showed no evidence of any dissolution [87]. In addition, Antia et al. [88] successfully observed that coccolith dissolution/fragmentation occurs inside zooplankton guts and microzooplankton vacuoles. During the first experiment, we observed a decoupling between ingestion rates (both pigment ingestion rates and equivalent volume ingestion rates) and fecal pellet egestion (Figure 3). Taking all the experiments collectively, this fact was also noticed in Experiment 5, with a high cell concentration of *E. huxleyi*. In addition, despite high measured ingestion rates, few fecal pellets were produced (Figures 5, 7 and 8). This decoupling between ingestion and egestion could be the result of a modulation of the residence time in the gut. Hence, fecal pellet size seems to depend on the ingestion rate index and prey quality (Figures 1, 6 and 8). Indeed, the fecal pellet size variation could depend on gut passage time as well [89]. By considering all these

points, both coccolithophore biovolume and relative calcite content may modulate coccolith dissolution due to gut passage variations.

4.4. Consequences for Vertical Particle Flux in the Pelagic Realm

In this study, we observed a loss of fecal pellet production with high prey concentrations, despite high ingestion rates. The number of egested particles (fecal pellets) seems to be dependant, not only on the food quantity, but also on the quality of the ingested food. The size of egested particles could be increased by both the number of ingested particles and their quality (inclusion of calcite, silica frustules, etc.). Prey/predator size ratio and relative carbon content [90] suggest that these environmental food conditions may provide predictable constraints to copepod biogeography size distribution in the ocean [91]. This therefore suggest that size and primary producer stoichiometry could influence oceanic carbon flux patterns through fecal pellet egestion by copepods. This may result in a decrease of carbon passive flux due to fecal pellets sinking in the water column. In addition, if we consider that fecal pellets follow Stoke's law of sedimentation (as suggested by Komar et al. [92]), the ballast effect of calcified coccoliths inside fecal pellets should foster the sedimentation rate much more than changes in the size of the pellets [93]. Hence, modification of fecal pellet egestion patterns in addition to ballast effect of calcite could be an important process driving the particle flux in the water column.

5. Conclusions

In this study, we demonstrated that copepod ingestion rates based on the volume equivalent of cells is better scaled to total prey volume concentration ($mm^3\ L^{-1}$). The Chl *a*/biovolume calibration developed in this study highlights the importance of considering the Chl *a* level inside the gut fluorescent content, regarding food types ingested by wild copepods, such as non-chlorophyllian preys (e.g., microzooplankton, heterotrophic flagelles, nauplii, etc.). Our results highlight an exponential increase of ingestion rates according to food availability (*Type III functional response*), which is in contrast to the optimal Ivlev model (*Type II functional response*) corresponding to optimal food foraging. This parametric pattern supports the role of food quality in the feeding behaviour of copepods, such as coccolithophore defence structures (calcified coccospheres). We demonstrated this aspect by showing the relationship between calcite content (PIC/POC ratio) and the ingestion rate index. Finally, we observed a decoupling between ingestion rates and fecal pellet egestion, which may be the consequence of an "obstruction" effect of calcite inside the copepod's gut. This "obstruction" may be the result of varying gut passage times—modulating the intensity of calcite dissolution. These results suggest that both prey allometry and stoichiometry need to be considered with copepod feeding dynamics, specifically regarding fecal pellet production, and the sedimentary flux, which is an important component of the biological carbon pump.

Author Contributions: Contributed to conception and design: J.T. and A.D. Contributed to acquisition of data: J.T., A.D., A.P. and G.D. Contributed to the copepod rearing maintenance: J.T., A.D. and A.P. Contributed to analysis and interpretation of data: J.T., A.D. and M.H. Drafted and/or revised the article: J.T., A.D. and M.H. Approved the submitted version for publication: J.T., A.D., A.P., G.D., V.C., L.B. and M.H. All authors have read and agreed to the published version of the manuscript.

Funding: This work was supported by the ANR CARCLIM (https://anr.fr/Projet-ANR-17-CE01-0004). Jordan Toullec's postdoctorate was equally funded by ANR CARCLIM and by Université Littoral Côte d'Opale. This work was also supported by the CPER MARCO and the SFR Campus de la Mer.

Institutional Review Board Statement: Not applicable.

Informed Consent Statement: Not applicable.

Data Availability Statement: All data are displayed within the manuscript or may be obtained directly from the authors.

Acknowledgments: We would like to thank the Sepia II crew for their help at sea, during zooplankton collection, and more specifically for the multiple WPII plankton hauls during *Phaeocystis globosa* sticky bloom event. We are also grateful to Michel Laréal for his help and modifications made to the rolling table.

Conflicts of Interest: The authors declare no conflict of interest.

References

1. Sanders, R.; Henson, S.A.; Koski, M.; De La Rocha, C.L.; Painter, S.C.; Poulton, A.J.; Riley, J.; Salihoglu, B.; Visser, A.; Yool, A.; et al. The Biological Carbon Pump in the North Atlantic. *Prog. Oceanogr.* **2014**, *129*, 200–218. [CrossRef]
2. Henson, S.; Le Moigne, F.; Giering, S. Drivers of Carbon Export Efficiency in the Global Ocean. *Glob. Biogeochem. Cycles* **2019**, *33*, 891–903. [CrossRef] [PubMed]
3. Le Moigne, F.A. Pathways of organic carbon downward transport by the oceanic biological carbon pump. *Front. Mar. Sci.* **2019**, *6*, 634. [CrossRef]
4. Turner, J.T. Zooplankton fecal pellets, marine snow, phytodetritus and the ocean's biological pump. *Prog. Oceanogr.* **2015**, *130*, 205–248. [CrossRef]
5. Steinberg, D.K.; Landry, M.R. Zooplankton and the Ocean Carbon Cycle. *Annu. Rev. Mar. Sci.* **2017**, *9*, 413–444. [CrossRef]
6. Laurenceau-Cornec, E.; Trull, T.W.; Davies, D.M.; Bray, S.G.; Doran, J.; Planchon, F.; Carlotti, F.; Jouandet, M.-P.; Cavagna, A.-J.; Waite, A.M.; et al. The relative importance of phytoplankton aggregates and zooplankton fecal pellets to carbon export: Insights from free-drifting sediment trap deployments in naturally iron-fertilised waters near the Kerguelen Plateau. *Biogeosciences* **2015**, *12*, 1007–1027. [CrossRef]
7. Belcher, A.; Iversen, M.; Manno, C.; Henson, S.A.; Tarling, G.A.; Sanders, R. The role of particle associated microbes in remineralization of fecal pellets in the upper mesopelagic of the Scotia Sea, Antarctica. *Limnol. Oceanogr.* **2016**, *61*, 1049–1064. [CrossRef]
8. Estapa, M.; Valdes, J.; Tradd, K.; Sugar, J.; Omand, M.; Buesseler, K. The neutrally buoyant sediment trap: Two decades of progress. *J. Atmos. Ocean. Technol.* **2020**, *37*, 957–973. [CrossRef]
9. Calbet, A. Mesozooplankton grazing effect on primary production: A global comparative analysis in marine ecosystems. *Limnol. Oceanogr.* **2001**, *46*, 1824–1830. [CrossRef]
10. Irigoien, X.; Harris, R.P.; Verheye, H.M.; Joly, P.; Runge, J.; Starr, M.; Pond, D.; Campbell, R.; Shreeve, R.; Ward, P.; et al. Copepod hatching success in marine ecosystems with high diatom concentrations. *Nature* **2002**, *419*, 387–389. [CrossRef]
11. Irigoien, X.; Flynn, K.J.; Harris, R.P. Phytoplankton blooms: A 'loophole' in microzooplankton grazing impact? *J. Plankton Res.* **2005**, *27*, 313–321. [CrossRef]
12. Brown, C.W.; Yoder, J.A. Coccolithophorid blooms in the global ocean. *J. Geophys. Res. Oceans* **1994**, *99*, 7467–7482. [CrossRef]
13. Eikrem, W.; Medlin, L.K.; Henderiks, J.; Rokitta, S.; Rost, B.; Probert, I.; Throndsen, J.; Edvardsen, B. Haptophyta. In *Handbook of the Protists*; Archibald, J.M., Simpson, A.G.B., Slamovits, C.H., Margulis, L., Melkonian, M., Chapman, D.J., Corliss, J.O., Eds.; Springer International Publishing: Cham, Switzerland, 2016; pp. 1–61. ISBN 978-3-319-32669-6.
14. Rost, B.; Riebesell, U. Coccolithophores and the biological pump: Responses to environmental changes. In *Coccolithophores*; Springer: Berlin/Heidelberg, Germany, 2004; pp. 99–125.
15. Henderiks, J.; Bartol, M.; Pige, N.; Karatsolis, B.-T.; Lougheed, B.C. Shifts in phytoplankton composition and stepwise climate change during the middle Miocene. *Paleoceanogr. Paleoclimatol.* **2020**, *35*, e2020PA003915. [CrossRef]
16. Hays, G.C.; Richardson, A.J.; Robinson, C. Climate change and marine plankton. *Trends Ecol. Evol.* **2005**, *20*, 337–344. [CrossRef]
17. Kléparski, L.; Beaugrand, G.; Edwards, M.; Schmitt, F.G.; Kirby, R.R.; Breton, E.; Gevaert, F.; Maniez, E. Morphological traits, niche-environment interaction and temporal changes in diatoms. *Prog. Oceanogr.* **2022**, *201*, 102747. [CrossRef]
18. Kiørboe, T.; Visser, A.W. Predator and prey perception in copepods due to hydromechanical signals. *Mar. Ecol. Prog. Ser.* **1999**, *179*, 81–95. [CrossRef]
19. Visser, A.W.; Fiksen, Ø. Optimal foraging in marine ecosystem models: Selectivity, profitability and switching. *Mar. Ecol. Prog. Ser.* **2013**, *473*, 91–101. [CrossRef]
20. Djeghri, N.; Atkinson, A.; Fileman, E.S.; Harmer, R.A.; Widdicombe, C.E.; McEvoy, A.J.; Cornwell, L.; Mayor, D.J. High prey-predator size ratios and unselective feeding in copepods: A seasonal comparison of five species with contrasting feeding modes. *Prog. Oceanogr.* **2018**, *165*, 63–74. [CrossRef]
21. Pančić, M.; Kiørboe, T. Phytoplankton defence mechanisms: Traits and trade-offs. *Biol. Rev.* **2018**, *93*, 1269–1303. [CrossRef]
22. Jansen, S. Copepods grazing on *Coscinodiscus wailesii*: A question of size? *Helgol. Mar. Res.* **2008**, *62*, 251–255. [CrossRef]
23. Friedrichs, L.; Hörnig, M.; Schulze, L.; Bertram, A.; Jansen, S.; Hamm, C. Size and biomechanic properties of diatom frustules influence food uptake by copepods. *Mar. Ecol. Prog. Ser.* **2013**, *481*, 41–51. [CrossRef]
24. Liu, H.; Chen, M.; Zhu, F.; Harrison, P.J. Effect of Diatom Silica Content on Copepod Grazing, Growth and Reproduction. *Front. Mar. Sci.* **2016**, *3*, 89. [CrossRef]
25. Pančić, M.; Torres, R.R.; Almeda, R.; Kiørboe, T. Silicified cell walls as a defensive trait in diatoms. *Proc. R. Soc. B Biol. Sci.* **2019**, *286*, 20190184. [CrossRef] [PubMed]

26. Xu, H.; Shi, Z.; Zhang, X.; Pang, M.; Pan, K.; Liu, H. Diatom frustules with different silica contents affect copepod grazing due to differences in the nanoscale mechanical properties. *Limnol. Oceanogr.* **2021**, *66*, 3408–3420. [CrossRef]
27. Zhang, S.; Liu, H.; Ke, Y.; Li, B. Effect of the Silica Content of Diatoms on Protozoan Grazing. *Front. Mar. Sci.* **2017**, *4*, 202. [CrossRef]
28. Pondaven, P.; Gallinari, M.; Chollet, S.; Bucciarelli, E.; Sarthou, G.; Schultes, S.; Jean, F. Grazing-induced Changes in Cell Wall Silicification in a Marine Diatom. *Protist* **2007**, *158*, 21–28. [CrossRef]
29. Petrucciani, A.; Chaerle, P.; Norici, A. Diatoms Versus Copepods: Could Frustule Traits Have a Role in Avoiding Predation? *Front. Mar. Sci.* **2022**, *8*, 804960. [CrossRef]
30. Jaya, B.N.; Hoffmann, R.; Kirchlechner, C.; Dehm, G.; Scheu, C.; Langer, G. Coccospheres confer mechanical protection: New evidence for an old hypothesis. *Acta Biomater.* **2016**, *42*, 258–264. [CrossRef]
31. Harvey, E.L.; Bidle, K.D.; Johnson, M.D. Consequences of strain variability and calcification in *Emiliania huxleyi* on microzooplankton grazing. *J. Plankton Res.* **2015**, *37*, 1137–1148. [CrossRef]
32. Mayers, K.M.J.; Poulton, A.J.; Bidle, K.; Thamatrakoln, K.; Schieler, B.; Giering, S.L.C.; Wells, S.R.; Tarran, G.A.; Mayor, D.; Johnson, M.; et al. The Possession of Coccoliths Fails to Deter Microzooplankton Grazers. *Front. Mar. Sci.* **2020**, *7*, 569896. [CrossRef]
33. Nejstgaard, J.C.; Gismervik, I.; Solberg, P.T. Feeding and reproduction by *Calanus finmarchicus*, and microzooplankton grazing during mesocosm blooms of diatoms and the coccolithophore *Emiliania huxleyi*. *Mar. Ecol. Prog. Ser.* **1997**, *147*, 197–217. [CrossRef]
34. Zondervan, I.; Zeebe, R.E.; Rost, B.; Riebesell, U. Decreasing marine biogenic calcification: A negative feedback on rising atmospheric pCO_2. *Glob. Biogeochem. Cycles* **2001**, *15*, 507–516. [CrossRef]
35. Monteiro, F.M.; Bach, L.T.; Brownlee, C.; Bown, P.; Rickaby, R.E.M.; Poulton, A.J.; Tyrrell, T.; Beaufort, L.; Dutkiewicz, S.; Gibbs, S.; et al. Why marine phytoplankton calcify. *Sci. Adv.* **2016**, *2*, e1501822. [CrossRef]
36. Kiørboe, T. How zooplankton feed: Mechanisms, traits and trade-offs. *Biol. Rev.* **2011**, *86*, 311–339. [CrossRef]
37. Kiørboe, T.; Møhlenberg, F.; Nicolajsen, H. Ingestion rate and gut clearance in the planktonic copepod *Centropages hamatus* (Lilljeborg) in relation to food concentration and temperature. *Ophelia* **1982**, *21*, 181–194. [CrossRef]
38. Ivlev, V.S. *Experimental Ecology of Nutrition of Fishes. Moscow, Pishchepromizdat. Translated by D. Scott*; Yale University Press: New Haven, CT, USA, 1955.
39. Kooij, R.E.; Zegeling, A. A Predator–Prey Model with Ivlev's Functional Response. *J. Math. Anal. Appl.* **1996**, *198*, 473–489. [CrossRef]
40. Stibor, H.; Vadstein, O.; Diehl, S.; Gelzleichter, A.; Hansen, T.; Hantzsche, F.; Katechakis, A.; Lippert, B.; Løseth, K.; Peters, C.; et al. Copepods act as a switch between alternative trophic cascades in marine pelagic food webs. *Ecol. Lett.* **2004**, *7*, 321–328. [CrossRef]
41. Moriceau, B.; Iversen, M.H.; Gallinari, M.; Evertsen, A.-J.O.; Le Goff, M.; Beker, B.; Boutorh, J.; Corvaisier, R.; Coffineau, N.; Donval, A.; et al. Copepods Boost the Production but Reduce the Carbon Export Efficiency by Diatoms. *Front. Mar. Sci.* **2018**, *5*, 82. [CrossRef]
42. Pan, Y.; Zhang, Y.; Sun, S. Phytoplankton–zooplankton dynamics vary with nutrients: A microcosm study with the cyanobacterium *Coleofasciculus chthonoplastes* and cladoceran *Moina micrura*. *J. Plankton Res.* **2014**, *36*, 1323–1332. [CrossRef]
43. Liu, Y.-W.; Rokitta, S.D.; Rost, B.; Eagle, R.A. Constraints on coccolithophores under ocean acidification obtained from boron and carbon geochemical approaches. *Geochim. Cosmochim. Acta* **2021**, *315*, 317–332. [CrossRef]
44. Besiktepe, S.; Dam, H. Coupling of ingestion and defecation as a function of diet in the calanoid copepod *Acartia tonsa*. *Mar. Ecol. Prog. Ser.* **2002**, *229*, 151–164. [CrossRef]
45. Butler, M.; Dam, H. Production rates and characteristics of fecal pellets of the copepod *Acartia tonsa* under simulated phytoplankton bloom conditions: Implications for vertical fluxes. *Mar. Ecol. Prog. Ser.* **1994**, *114*, 81–91. [CrossRef]
46. Keller, M.D.; Selvin, R.C.; Claus, W.; Guillard, R.R.L. Media for the Culture of Oceanic Ultraphytoplankton 1, 2. *J. Phycol.* **1987**, *23*, 633–638. [CrossRef]
47. Aminot, A.; Kérouel, R. *Hydrologie des Écosystèmes Marins: Paramètres et Analyses*; Editions Quae: Versailles, France, 2004; ISBN 978-2-84433-133-5.
48. Seuront, L.; Vincent, D. Increased seawater viscosity, *Phaeocystis globosa* spring bloom and *Temora longicornis* feeding and swimming behaviours. *Mar. Ecol. Prog. Ser.* **2008**, *363*, 131–145. [CrossRef]
49. Benedetti, F.; Gasparini, S.; Ayata, S.-D. Identifying copepod functional groups from species functional traits. *J. Plankton Res.* **2016**, *38*, 159–166. [CrossRef]
50. Lombard, F.; Koski, M.; Kiørboe, T. Copepods use chemical trails to find sinking marine snow aggregates. *Limnol. Oceanogr.* **2013**, *58*, 185–192. [CrossRef]
51. Vincent, D.; Slawyk, G.; L'Helguen, S.; Sarthou, G.; Gallinari, M.; Seuront, L.; Sautour, B.; Ragueneau, O. Net and gross incorporation of nitrogen by marine copepods fed on ^{15}N-labelled diatoms: Methodology and trophic studies. *J. Exp. Mar. Biol. Ecol.* **2007**, *352*, 295–305. [CrossRef]
52. Toullec, J.; Vincent, D.; Frohn, L.; Miner, P.; Le Goff, M.; Devesa, J.; Moriceau, B. Copepod Grazing Influences Diatom Aggregation and Particle Dynamics. *Front. Mar. Sci.* **2019**, *6*, 751. [CrossRef]
53. Berggreen, U.; Hansen, B.; Kiørboe, T. Food size spectra, ingestion and growth of the copepod *Acartia tonsa* during development: Implications for determination of copepod production. *Mar. Biol.* **1988**, *99*, 341–352. [CrossRef]

54. Bonnet, D.; Titelman, J.; Harris, R. *Calanus* the cannibal. *J. Plankton Res.* **2004**, *26*, 937–948. [CrossRef]
55. Boersma, M.; Wesche, A.; Hirche, H.-J. Predation of calanoid copepods on their own and other copepods' offspring. *Mar. Biol.* **2014**, *161*, 733–743. [CrossRef]
56. Schultes, S.; Sourisseau, M.; Le Masson, E.; Lunven, M.; Marié, L. Influence of physical forcing on mesozooplankton communities at the Ushant tidal front. *J. Mar. Syst.* **2013**, *109–110*, S191–S202. [CrossRef]
57. Grattepanche, J.-D.; Breton, E.; Brylinski, J.-M.; Lecuyer, E.; Christaki, U. Succession of primary producers and micrograzers in a coastal ecosystem dominated by *Phaeocystis globosa* blooms. *J. Plankton Res.* **2011**, *33*, 37–50. [CrossRef]
58. Sautour, B.; Castel, J. Feeding behaviour of the coastal copepod *Euterpina acutifrons* on small particles. *Cah Biol Mar* **1993**, *34*, 239–251.
59. Vincent, D.; Hartmann, H.J. Contribution of ciliated microprotozoans and dinoflagellates to the diet of three copepod species in the Bay of Biscay. *Hydrobiologia* **2001**, *443*, 193–204. [CrossRef]
60. Sarthou, G.; Vincent, D.; Christaki, U.; Obernosterer, I.; Timmermans, K.R.; Brussaard, C.P. The fate of biogenic iron during a phytoplankton bloom induced by natural fertilisation: Impact of copepod grazing. *Deep Sea Res. Part II Top. Stud. Oceanogr.* **2008**, *55*, 734–751. [CrossRef]
61. Durbin, E.G.; Campbell, R.G. Reassessment of the gut pigment method for estimating in situ zooplankton ingestion. *Mar. Ecol. Prog. Ser.* **2007**, *331*, 305–307. [CrossRef]
62. Dam, H.G.; Peterson, W.T. The effect of temperature on the gut clearance rate constant of planktonic copepods. *J. Exp. Mar. Biol. Ecol.* **1988**, *123*, 1–14. [CrossRef]
63. Jeschke, J.M.; Kopp, M.; Tollrian, R. Consumer-food systems: Why type I functional responses are exclusive to filter feeders. *Biol. Rev.* **2004**, *79*, 337–349. [CrossRef]
64. Kiørboe, T.; Saiz, E.; Tiselius, P.; Andersen, K.H. Adaptive feeding behavior and functional responses in zooplankton. *Limnol. Oceanogr.* **2018**, *63*, 308–321. [CrossRef]
65. Hillebrand, H.; Dürselen, C.-D.; Kirschtel, D.; Pollingher, U.; Zohary, T. Biovolume calculation for pelagic and benthic microalgae. *J. Phycol.* **1999**, *35*, 403–424. [CrossRef]
66. Villiot, N.; Poulton, A.J.; Butcher, E.T.; Daniels, L.R.; Coggins, A. Allometry of carbon and nitrogen content and growth rate in a diverse range of coccolithophores. *J. Plankton Res.* **2021**, *43*, 511–526. [CrossRef]
67. Menden-Deuer, S.; Lessard, E.J. Carbon to volume relationships for dinoflagellates, diatoms, and other protist plankton. *Limnol. Oceanogr.* **2000**, *45*, 569–579. [CrossRef]
68. Holling, C.S. The Functional Response of Predators to Prey Density and its Role in Mimicry and Population Regulation. *Memoirs Èntomol. Soc. Can.* **1965**, *97*, 5–60. [CrossRef]
69. Murdoch, W.W. Stabilizing effects of spatial heterogeneity in predator-prey systems. *Theor. Popul. Biol.* **1977**, *11*, 252–273. [CrossRef]
70. Cavan, E.L.; Henson, S.A.; Belcher, A.; Sanders, R. Role of zooplankton in determining the efficiency of the biological carbon pump. *Biogeosciences* **2017**, *14*, 177–186. [CrossRef]
71. Belcher, A.; Manno, C.; Ward, P.; Henson, S.A.; Sanders, R.; Tarling, G.A. Copepod faecal pellet transfer through the meso- and bathypelagic layers in the Southern Ocean in spring. *Biogeosciences* **2017**, *14*, 1511–1525. [CrossRef]
72. Prowe, A.E.F.; Pahlow, M.; Dutkiewicz, S.; Follows, M.; Oschlies, A. Top-down control of marine phytoplankton diversity in a global ecosystem model. *Prog. Oceanogr.* **2012**, *101*, 1–13. [CrossRef]
73. Wang, R.; Conover, R.J. Dynamics of gut pigment in the copepod Temora longicornis and the determination of in situ grazing rates. *Limnol. Oceanogr.* **1986**, *31*, 867–877. [CrossRef]
74. Kiørboe, T.; Tiselius, P.T. Gut clearance and pigment destruction in a herbivorous copepod, Acartia tonsa, and the determi-nation of in situ grazing rates. *J. Plankton Res.* **1987**, *9*, 525–534. [CrossRef]
75. Jansen, S.; Bathmann, U. Algae viability within copepod faecal pellets: Evidence from microscopic examinations. *Mar. Ecol. Prog. Ser.* **2007**, *337*, 145–153. [CrossRef]
76. Agustí, S.; González-Gordillo, J.I.; Vaqué, D.; Estrada, M.; Cerezo, M.I.; Salazar, G.; Gasol, J.M.; Duarte, C.M. Ubiquitous healthy diatoms in the deep sea confirm deep carbon injection by the biological pump. *Nat. Commun.* **2015**, *6*, 7608. [CrossRef] [PubMed]
77. Harris, R.P.; Paffenhöfer, G.-A. Feeding, growth and reproduction of the marine planktonic copepod *Temora longicornis* Müller. *J. Mar. Biol. Assoc. UK* **1976**, *56*, 675–690. [CrossRef]
78. Price, H.J.; Paffenhöfer, G.-A. Effects of concentration on the feeding of a marine copepod in algal monocultures and mixtures. *J. Plankton Res.* **1986**, *8*, 119–128. [CrossRef]
79. Harris, R.P. Zooplankton grazing on the coccolithophore *Emiliania huxleyi* and its role in inorganic carbon flux. *Mar. Biol.* **1994**, *119*, 431–439. [CrossRef]
80. Tirelli, V.; Mayzaud, P. Relationship between functional response and gut transit time in the calanoid copepod *Acartia clausi*: Role of food quantity and quality. *J. Plankton Res.* **2005**, *27*, 557–568. [CrossRef]
81. Milliman, J.D.; Troy, P.J.; Balch, W.M.; Adams, A.K.; Li, Y.-H.; Mackenzie, F.T. Biologically mediated dissolution of calcium carbonate above the chemical lysocline? *Deep Sea Res. Part Oceanogr. Res. Pap.* **1999**, *46*, 1653–1669. [CrossRef]
82. Roth, P.H.; Mullin, M.M.; Berger, W.H. Coccolith Sedimentation by Fecal Pellets: Laboratory Experiments and Field Observations. *GSA Bull.* **1975**, *86*, 1079–1084. [CrossRef]
83. Honjo, S. Coccoliths: Production, transportation and sedimentation. *Mar. Micropaleontol.* **1976**, *1*, 65–79. [CrossRef]

84. Honjo, S.; Roman, M.R. Marine copepod fecal pellets: Production, preservation and sedimentation. *J Mar Res* **1978**, *36*, 45–57.
85. Samtleben, C.; Bickert, T. Coccoliths in sediment traps from the Norwegian Sea. *Mar. Micropaleontol.* **1990**, *16*, 39–64. [CrossRef]
86. Jansen, H.; Wolf-Gladrow, D.A. Carbonate dissolution in copepod guts: A numerical model. *Mar. Ecol. Prog. Ser.* **2001**, *221*, 199–207. [CrossRef]
87. Langer, G.; Nehrke, G.; Jansen, S. Dissolution of *Calcidiscus leptoporus* coccoliths in copepod guts? A morphological study. *Mar. Ecol. Prog. Ser.* **2007**, *331*, 139–146. [CrossRef]
88. Antia, A.N.; Suffrian, K.; Holste, L.; Müller, M.N.; Nejstgaard, J.C.; Simonelli, P.; Carotenuto, Y.; Putzeys, S. Dissolution of coccolithophorid calcite by microzooplankton and copepod grazing. *Biogeosci. Discuss.* **2008**, *5*, 1–23.
89. Wilson, S.E.; Steinberg, D.K.; Buesseler, K.O. Changes in fecal pellet characteristics with depth as indicators of zooplankton repackaging of particles in the mesopelagic zone of the subtropical and subarctic North Pacific Ocean. *Deep Sea Res. Part II Top. Stud. Oceanogr.* **2008**, *55*, 1636–1647. [CrossRef]
90. Almeda, R.; Someren Gréve, H.; Kiørboe, T. Prey perception mechanism determines maximum clearance rates of planktonic copepods. *Limnol. Oceanogr.* **2018**, *63*, 2695–2707. [CrossRef]
91. Beaugrand, G.; Reid, P.C.; Ibañez, F.; Lindley, J.A.; Edwards, M. Reorganization of North Atlantic Marine Copepod Biodiversity and Climate. *Science* **2002**, *296*, 1692–1694. [CrossRef]
92. Komar, P.D.; Morse, A.P.; Small, L.F.; Fowler, S.W. An analysis of sinking rates of natural copepod and euphausiid fecal pellets 1. *Limnol. Oceanogr.* **1981**, *26*, 172–180. [CrossRef]
93. White, M.M.; Waller, J.D.; Lubelczyk, L.C.; Drapeau, D.T.; Bowler, B.C.; Balch, W.M.; Fields, D.M. Coccolith dissolution within copepod guts affects fecal pellet density and sinking rate. *Sci. Rep.* **2018**, *8*, 9758. [CrossRef]